

Motion Planning and Collision Avoidance using Non-Gradient Vector Fields

Dimitra Panagou

Abstract

This paper presents a novel feedback method on the motion planning for unicycle robots in environments with static obstacles, along with an extension to the distributed planning and coordination in multi-robot systems. The method employs a family of 2-dimensional analytic vector fields, whose integral curves exhibit various patterns depending on the value of a parameter λ . More specifically, for an a priori known value of λ , the vector field has a unique singular point of dipole type and can be used to steer the unicycle to a goal configuration. Furthermore, for the unique value of λ that the vector field has a continuum of singular points, the integral curves are used to define flows around obstacles. An almost global feedback motion plan can then be constructed by suitably blending attractive and repulsive vector fields in a static obstacle environment. The method does not suffer from the appearance of sinks (stable nodes) away from goal point. Compared to other similar methods which are free of local minima, the proposed approach does not require any parameter tuning to render the desired convergence properties. The paper also addresses the extension of the method to the distributed coordination and control of multiple robots, where each robot needs to navigate to a goal configuration while avoiding collisions with the remaining robots, and while using local information only. More specifically, based on the results which apply to the single-robot case, a motion coordination protocol is presented which guarantees the safety of the multi-robot system and the almost global convergence of the robots to their goal configurations. The efficacy of the proposed methodology is demonstrated via simulation results in static and dynamic environments.

I. INTRODUCTION

Motion planning, coordination and control for robotic systems still remains an active research topic in many respects. The primary motivation has been the computation of safe, collision-free

Dimitra Panagou is with the Department of Aerospace Engineering, University of Michigan, Ann Arbor, MI, USA; dpanagou@umich.edu.

trajectories for robotic agents, mechanisms and autonomous vehicles which operate in constrained and/or uncertain environments. Research within the robotics community has attributed various formulations and methodologies on the motion planning problem, often specialized based on the control objectives and the characteristics of the problems at hand. These methodologies range from Lyapunov-based control methods, to sampling-based planning, to combinatorial planning, to formal methods [1]–[3]. Multi-robot systems have attracted the interest of the control systems community as well. Emphasis has been given in consensus, flocking and formation control problems for multiple agents [4].

Avoiding obstacles and inter-agent collisions is a requirement of highest priority in motion planning and coordination problems. Recently, significant interest has been paid to the high-level task planning under complex goals, where the problem for an autonomous robot has transitioned from the classical motion planning formulation (i.e., move from point A to point B) to the consideration of complex goals under temporal specifications; such specifications are typically described as: “visit region A , and then visit either region B or region C ”. Despite the tremendous and elegant contributions in this area, which provide elegant solutions to the high-level mission synthesis with rigorous guarantees under certain assumptions on the considered environments [2], [3], the interconnection of high-level tasking with the physical layer/system is still an open problem in many respects. One issue is the consideration of multiple agents in dynamic environments and the associated complexity in finding provably correct solutions in the presence of nonlinearities, arbitrary constraints, and uncertainty.

The scope of this paper is to provide a solution to the motion planning problem for single and multiple nonholonomic agents in dynamic environments, where agents have local sensing and communication capabilities and which may be populated by dynamic (moving) obstacles. Our goal is to provide a feedback synthesis of low-level planning controllers along with certain guarantees, which can later on be combined with high-level tasks, such as dynamic coverage [5], towards provably correct feedback solutions for a specific class of dynamical systems in dynamic environments. The technical tools which we use towards this goal are set-invariance methods, which have been proved efficient in constrained control problems of a class of nonlinear, under-actuated systems [6].

The spirit of the proposed solutions is similar, *but not identical to*, Lyapunov-like scalar functions, such as the Avoidance Functions in [7] and the Artificial Potential Fields (APF) in

[8], [9]. More specifically: It is well-known that, although scalar functions offer the merit of Lyapunov-based control design and analysis, yielding thus solutions in closed-form with certain guarantees [10], they suffer from the drawback of possible local minima away from the goal point, i.e., of points in the state space other than the desired equilibrium at which the gradient vector vanishes; this in principle results in system trajectories which get stuck away from the goal point. Certain forms of potential functions may overcome this limitation; namely, navigation functions [11] and harmonic functions [12], [13], but under some cost: the caveat in the former case is that the Morse property which guarantees the non-existence of local minima is rendered after a tuning parameter exceeds a lower bound, which is not a priori known. In the latter case, harmonic functions may be constructed with either discrete or continuous approaches, but the computational cost of discrete methods is quite demanding. Continuous approaches which employ the analogies of Laplace equation with fluid mechanics yield closed-form solutions for certain dynamic environments [14]. Stream functions [15] combine the local-minima-free property of harmonic functions along with hydrodynamic concepts to yield streamlines which may be preferable for second order systems. The method of vortex fields [16] uses the anti-gradient of a scalar function to define flows around obstacles.

Now, let us note that one common ground in this class of solutions is the resulting *gradient vector field* which is employed in the control synthesis. In this respect, the idea of *directly* defining vector fields encoding obstacle avoidance has been studied for robot motion planning problems. In [17], for instance, simple smooth vector fields are locally constructed in given convex cell decompositions of polygonal environments, so that their integral curves are by construction collision-free and, in a sequential composition spirit, convergent to a goal point. The method, nevertheless, presumes the existence of a high-level discrete motion plan which determines the successive order of the cells from an initial to a final configuration. Recent work employing vector fields for vehicles' navigation is presented also in [18] and in [19]. The approach with velocity vector fields in [20] is also relevant to the context. However, these contributions address only the position control of the robot, while the orientation is not guaranteed to converge to a desired value.

Stepping now a little further away from single-agent problems: when it comes to multiple agents, their motion towards goal configurations defines a dynamic environment and poses challenges to the planning, coordination and control design, even in the absence of static physical

obstacles. At the same time, limitations in the available sensing and communication platforms impose additional constraints to the multi-agent system. Given a pair (i, j) of agents i and j , agents typically make decisions on their actions based on available information, which can be either locally measured using onboard sensors, or transmitted and received across the nodes of the multi-agent system via wireless communication links. Thus, information flow between two agents can be either bidirectional (undirected) or unidirectional (directed). During the past ten years, research efforts have achieved the formalization of problems such as consensus and formation control in multi-agent networks using tools and notions from graph theory, matrix theory and Lyapunov stability theory [21]–[25]. The case of directed information exchange has recently attracted increased interest [26]–[30], motivated in part by the fact that undirected information flow is not always a realistic and practical assumption, due to bandwidth limitations in the network, anisotropic sensing of the agents etc. Extending consensus algorithms to nonlinear systems has also become popular, see for instance [31], [32].

Nevertheless, despite that consensus, flocking, and formation control algorithms achieve collision avoidance in multi-vehicle systems by carefully selecting initial conditions and controlling relative distance and heading, they are typically not used in encoding problems such as navigation to *specific* goal locations for each one of the agents. In this respect, the development of planning and coordination algorithms for the motion of multiple agents along with safety and performance guarantees is an open problem in many respects.

A. Overview

This paper presents a novel method on the motion planning and coordination in environments with static and/or dynamic obstacles, which results in feedback motion plans for unicycle robots along with collision avoidance guarantees. The method employs a family of two-dimensional analytic vector fields, originally introduced in [33], given as:

$$\mathbf{F}(\mathbf{r}) = \lambda(\mathbf{p}^T \mathbf{r})\mathbf{r} - \mathbf{p}(\mathbf{r}^T \mathbf{r}), \quad (1)$$

where $\lambda \in \mathbb{R}$ is a parameter to be specified later on, $\mathbf{r} = [x \ y]^T$ the position vector with respect to (w.r.t.) a global cartesian frame and $\mathbf{p} = [p_x \ p_y]^T$, with $\mathbf{p} \neq \mathbf{0}$.¹

¹The role the vector $\mathbf{p} \in \mathbb{R}^2$ plays in the properties of the vector field (1) becomes evident later on in Theorem 2.

In [33] the family of vector fields (1) was employed in the control design for steering kinematic, drift-free systems in chained form in *obstacle-free* environments.

In this paper we first show that, except for a *known* value of the parameter λ , the vector field (1) has a unique singular point on \mathbb{R}^2 . More specifically: (i) For $\lambda > 1$ the pattern of the integral curves around the unique singular point is dipolar [34]. Such vector field can be used for steering a unicycle to a goal configuration. (ii) For $\lambda = 1$ the vector field has a continuum of singular points and can be used to define tangential flows around circular obstacles. (iii) For $\lambda < 0$ the pattern of the integral curves is suitable for defining repulsive flows away from lines, and as thus, away from polygonal obstacles. A preliminary example is given in the Appendix of [35].

We then consider the single-agent case in a static environment of circular obstacles and propose a blending mechanism between attractive and repulsive vector fields, which yields almost global feedback motion plans. In other words, we construct vector fields whose integral curves are convergent to a goal configuration, except for a set of initial conditions of Lebesgue measure zero, and collision-free by construction. This in turn results in simple feedback control laws, which force the system to flow along the vector field.

We finally consider the extension of the methodology to the distributed coordination and control for multiple nonholonomic agents. Based on the results for the single-agent case in static obstacle environments, we propose a coordination protocol for multiple agents which need to converge to specific goal configurations, using local information only. The proposed protocol yields collision-free and almost globally convergent trajectories for the multi-agent system.

B. Contributions and Organization

When it comes to the single-agent case, i.e., to a robot operating in a known, static environment of circular obstacles, the proposed method does not suffer from the appearance of sinks (stable nodes) away from goal point. Furthermore, compared to similar feedback methods which rely on scalar (potential) functions, such as [11], the main difference and advantage of the proposed approach is that:

- (i) no parameter tuning is needed in order to render the desired convergence properties; the values of the parameter λ of the vector field are known *a priori*.

Compared to similar methods which rely on vector fields, such as [17], the proposed method:

- (ii) requires neither the computation of a cell decomposition of the free space, nor the existence of a high-level discrete motion plan, and as thus it is free of any computational complexity issues,
- (iii) addresses the motion planning and collision avoidance for multiple agents in dynamic environments, and is scalable as the number of agents increases.

Finally, compared to other similar vector field based methods, such as [18]–[20], the proposed method:

- (iv) guarantees the convergence of the orientation trajectories of the robots to any predefined value.

Remark 1: While here we consider circular, not polygonal, obstacle environments, preliminary results reveal that the method can be used for defining repulsions around polygonal obstacles as well, see the Appendix in [35].

When it comes to the multi-agent case, i.e., to multiple agents moving towards goal configurations while avoiding collisions, the proposed method:

- (v) offers the flexibility to directly impose the minimum allowable clearance among agents, something which typically is not the case with gradient-based solutions. This characteristic might be desirable, for instance, when considering multi-robot systems in confined environments.
- (vi) being a non-gradient vector field approach, the technical developments are based on set invariance concepts rather than Lyapunov-based methods. This in principle provides less conservative solutions, while it might be desirable in extending the method to more complicated dynamical models.

Compared to our earlier work, the vector field construction presented here is not the same with the one in [36]. Furthermore, the proposed construction, coordination protocol and technical developments are not the same with the ones in [37]. Moreover, since it offers feedback solutions with certain convergence guarantees, it can be used as a basis in constrained model predictive control designs [38], which are appropriate for uncertain environments. The case of mixed environments, i.e., of multiple agents operating among physical obstacles under uncertainty, are not considered in this paper and this topic is left open for future research.

Part of this work has appeared in [39]. The current paper additionally includes: (i) a detailed presentation of the overall method both for the static and the dynamic case, along with the proofs which have been omitted in the conference version in the interest of space, (ii) more simulation results which demonstrate the efficacy of the method in static and dynamic environments.

The paper is organized as follows: Section II includes a brief overview of the notions regarding the topology of two-dimensional vector fields that are used throughout the paper. Section III characterizes the singular points of our vector fields w.r.t. the parameter λ , while section IV presents the blending mechanism among vector fields, the construction of the almost global feedback motion plans and the underlying control design, along with simulation results in static obstacle environments. Section V presents the extension of the method to the distributed coordination and collision-free motion of multiple agents under various sensing/communication patterns. Our conclusions and thoughts on future work are summarized in Section VI.

II. SINGULAR POINTS OF VECTOR FIELDS

This section provides an overview of notions from vector field topology. For more information the reader is referred to [34], [40], [41].

Definition 1: A vector field on an open subset $U \subset \mathbb{R}^n$ is a function which assigns to each point $p \in U$ a vector $X_p \in T_p(\mathbb{R}^n)$. A vector field on \mathbb{R}^n is C^∞ (smooth) if its components relative to the canonical basis are C^∞ functions on U .

Definition 2: Given a C^∞ vector field X on \mathbb{R}^n , a curve $t \rightarrow F(t)$ defined on an open interval J of \mathbb{R} is an integral curve of X if $\frac{dF}{dt} = X_{F(t)}$ on J .

Definition 3: A point p of U at which $X_p = 0$ is called a singular, or critical, point of the vector field.

Center-type and non-center type singularities: Singular points are typically distinguished to those that are reached by no integral curve (called *center* type) and those that are reached by at least two integral curves (called *non-center* type). In the case of a center type singularity, one can find a neighborhood of the singular point where all integral curves are closed, inside one another, and contain the singular point into their interior. In the case of non-center type singularities, one has that at least two integral curves converge to the singular point. The local structure of a non-center type singularity is analyzed by considering the behavior of all the integral curves which pass through the neighborhood of the singular point. This neighborhood

is made of several curvilinear sectors. A curvilinear sector is defined as the region bounded by a circle C of arbitrary small radius, and two integral curves, S and S' , which both converge (for either $t \rightarrow +\infty$, or $t \rightarrow -\infty$) to the singular point. The integral curves passing through the open sector g (i.e., the integral curves except for S, S') determine the following three possible types of curvilinear sectors [42]: (i) *Elliptic* sectors: all integral curves begin and end at the critical point. (ii) *Parabolic* sectors: just one end of each integral curve is at the critical point. (iii) *Hyperbolic* sectors: the integral curves do not reach the critical point at all. The integral curves that separate each sector from the next are called separatrixes, see also Fig. 1.

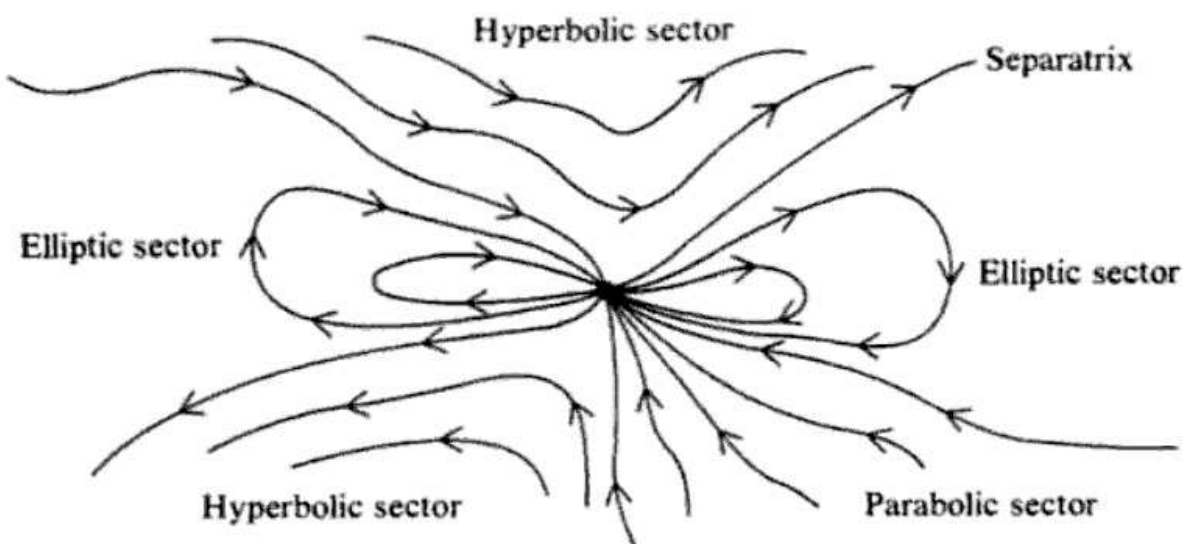


Fig. 1. A typical isolated critical point. Image taken from [34].

First-order and high-order singularities: A singular point p of a vector field X on \mathbb{R}^2 is called a *first-order* singular point if the Jacobian matrix $\mathbf{J}_X(\cdot)$ of the vector field X does not vanish (i.e., is nonsingular) on p , i.e., if: $\det(\mathbf{J}_X(p)) \neq 0$; otherwise the singular point is called *high-order* singular point.

III. NAVIGATION VIA VECTOR FIELDS

Consider the motion of a robot with unicycle kinematics in an environment \mathcal{W} with N static obstacles. The equations of motion read:

$$\begin{bmatrix} \dot{x} \\ \dot{y} \\ \dot{\theta} \end{bmatrix} = \begin{bmatrix} \cos \theta & 0 \\ \sin \theta & 0 \\ 0 & 1 \end{bmatrix} \begin{bmatrix} u \\ \omega \end{bmatrix}, \quad (2)$$

where $\mathbf{q} = [\mathbf{r}^T \ \theta]^T$ is the configuration vector, $\mathbf{r} = [x \ y]^T$ is the position and θ is the orientation of the robot w.r.t. a global frame \mathcal{G} , and u, ω are the linear and the angular velocity of the robot, respectively. The robot is modeled as a closed circular disk of radius ϱ , and each obstacle \mathcal{O}_i is modeled as a closed circular disk of radius ϱ_{oi} centered at $\mathbf{r}_{oi} = [x_{oi} \ y_{oi}]^T$, $i \in \{1, \dots, N\}$. Denote $\mathcal{O}_i = \{\mathbf{r} \in \mathbb{R}^2 \mid \|\mathbf{r} - \mathbf{r}_{oi}\| \leq \varrho_{oi}\}$.

A. A family of vector fields for robot navigation

We consider the class of vector fields $\mathbf{F} : \mathbb{R}^2 \rightarrow \mathbb{R}^2$ given by (1). The vector field components F_x, F_y read:

$$F_x = (\lambda - 1)p_x x^2 + \lambda p_y xy - p_x y^2, \quad (3a)$$

$$F_y = (\lambda - 1)p_y y^2 + \lambda p_x xy - p_y x^2. \quad (3b)$$

Theorem 1: The origin $\mathbf{r} = \mathbf{0}$ is the unique singular point of the vector field \mathbf{F} (1) if and only if $\lambda \neq 1$.

Proof: It is straightforward to verify that $\mathbf{r} = \mathbf{0}$ is a singular point of \mathbf{F} . Let us write the vector field components (3) of \mathbf{F} in matrix form as:

$$\begin{bmatrix} F_x \\ F_y \end{bmatrix} = \underbrace{\begin{bmatrix} (\lambda - 1)x^2 - y^2 & \lambda xy \\ \lambda xy & (\lambda - 1)y^2 - x^2 \end{bmatrix}}_{\mathbf{A}(\lambda, \mathbf{r})} \begin{bmatrix} p_x \\ p_y \end{bmatrix}. \quad (4)$$

The determinant of the matrix $\mathbf{A}(\lambda, \mathbf{r})$ is: $\det(\mathbf{A}(\lambda, \mathbf{r})) = -(\lambda - 1)(x^2 + y^2)^2$. This implies that $\mathbf{A}(\lambda, \mathbf{r})$ is nonsingular away from the origin $\mathbf{r} = \mathbf{0}$ if and only if $\lambda \neq 1$. Therefore, for $\lambda \neq 1$ and $\mathbf{r} \neq \mathbf{0}$, one has $\mathbf{F} = \mathbf{0}$ if and only if $\mathbf{p} = \mathbf{0}$. Since $\mathbf{p} \neq \mathbf{0}$ by definition, it follows that the vector field \mathbf{F} is nonsingular everywhere but the origin $\mathbf{r} = \mathbf{0}$, as long as $\lambda \neq 1$. ■

Theorem 2: The line $l : y = \tan \varphi x$, where $\tan \varphi \triangleq \frac{p_y}{p_x}$, is an axis of reflection, or mirror line, for \mathbf{F} (1).

Proof: Consider two points A, B of equal distance and on opposite sides w.r.t. the line l (Fig. 2). Their position vectors $\mathbf{r}_A = [x_A \ y_A]^T$, $\mathbf{r}_B = [x_B \ y_B]^T$ w.r.t. \mathcal{G} read:

$$x_A = R \cos a, \quad y_A = R \sin a, \quad (5a)$$

$$x_B = R \cos(2\varphi - a), \quad y_B = R \sin(2\varphi - a), \quad (5b)$$

where (R, a) , $(R, (2\varphi - a))$ are the polar coordinates of A, B , respectively. We need to prove

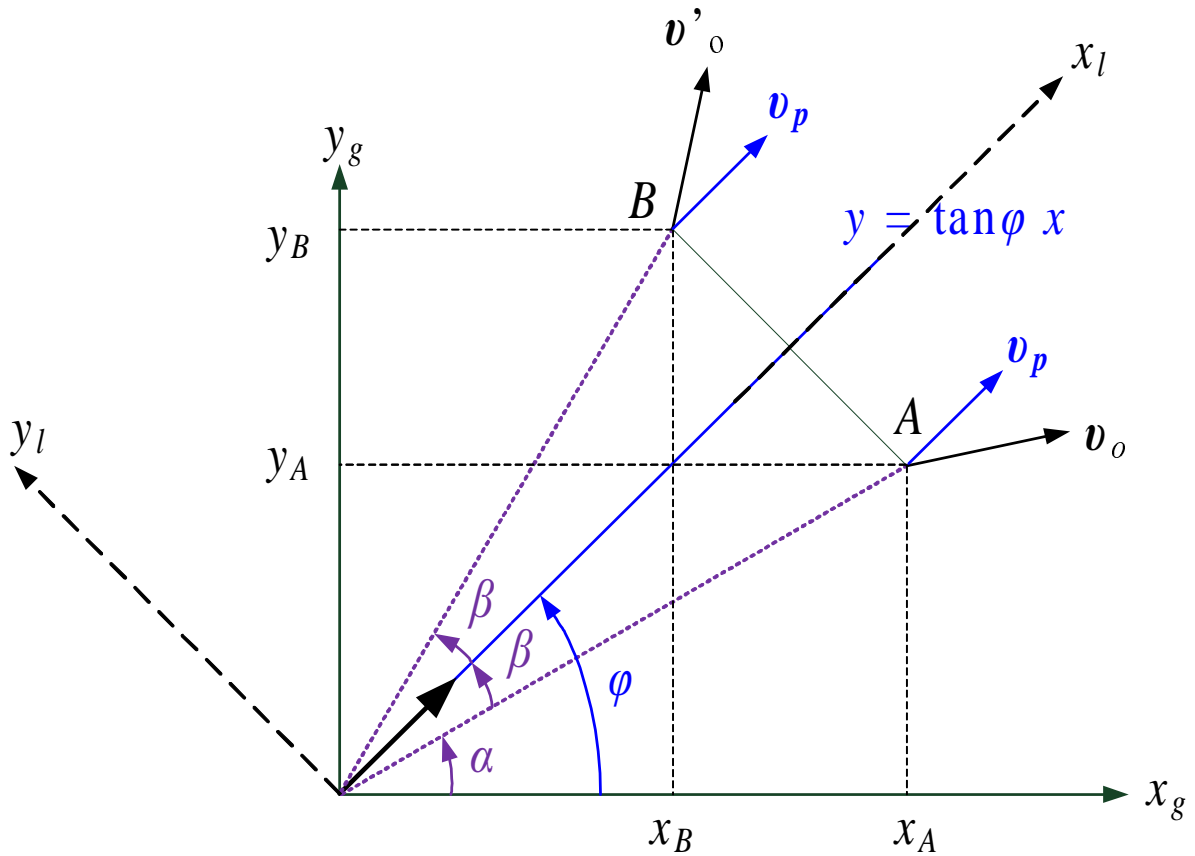


Fig. 2. The line $l : y = \tan \varphi x$, where $\varphi = \arctan(\frac{p_y}{p_x})$, is a reflection (or mirror) line for the vector field \mathbf{F} .

that the vector $\mathbf{F}(\mathbf{r}_A)$, denoted \mathbf{F}_A , reflects to the vector $\mathbf{F}(\mathbf{r}_B)$, denoted \mathbf{F}_B , w.r.t. the line $l : y = \tan \varphi x$. Recall that the reflection matrix about the considered line l is:

$$\mathbf{H}(2\varphi) = \begin{bmatrix} \cos 2\varphi & \sin 2\varphi \\ \sin 2\varphi & -\cos 2\varphi \end{bmatrix}. \quad (6)$$

Substituting (5a) into (4) and after some standard algebra yields:

$$\mathbf{F}_A = \underbrace{\frac{(\lambda - 2)R^2\|\mathbf{p}\|}{2} \begin{bmatrix} \cos \varphi \\ \sin \varphi \end{bmatrix}}_{\mathbf{v}_p} + \underbrace{\frac{\lambda R^2\|\mathbf{p}\|}{2} \begin{bmatrix} \cos(\varphi - 2a) \\ -\sin(\varphi - 2a) \end{bmatrix}}_{\mathbf{v}_o}, \quad (7)$$

where $\|\mathbf{p}\| = \sqrt{p_x^2 + p_y^2}$. Similarly, substituting (5b) into (4) yields:

$$\mathbf{F}_B = \underbrace{\frac{(\lambda - 2)R^2\|\mathbf{p}\|}{2} \begin{bmatrix} \cos \varphi \\ \sin \varphi \end{bmatrix}}_{\mathbf{v}_p} + \underbrace{\frac{\lambda R^2\|\mathbf{p}\|}{2} \begin{bmatrix} \cos 2\varphi & \sin 2\varphi \\ \sin 2\varphi & -\cos 2\varphi \end{bmatrix} \begin{bmatrix} \cos(\varphi - 2a) \\ -\sin(\varphi - 2a) \end{bmatrix}}_{\mathbf{v}'_o}. \quad (8)$$

One has: $\mathbf{F}_A = \mathbf{v}_p + \mathbf{v}_o$ and $\mathbf{F}_B = \mathbf{v}_p + \mathbf{v}'_o$. Out of (7), (8) one gets that $\mathbf{v}'_o = \mathbf{H}(2\varphi)\mathbf{v}_o$, i.e., \mathbf{v}'_o is the reflection of the vector \mathbf{v}_o about the line l . Thus, one may write

$$\mathbf{v}_o = v_{ox}^l \hat{\mathbf{x}}_l + v_{oy}^l \hat{\mathbf{y}}_l \quad \text{and} \quad \mathbf{v}'_o = v_{ox}^l \hat{\mathbf{x}}_l - v_{oy}^l \hat{\mathbf{y}}_l,$$

where $\hat{\mathbf{x}}_l, \hat{\mathbf{y}}_l$ are the unit vectors along the axes x_l, y_l , respectively, see Fig. 2. Furthermore, \mathbf{v}_p is parallel to the vector \mathbf{p} , i.e., parallel to the candidate reflection line l . Consequently, one may write: $\mathbf{v}_p = v_{px}^l \hat{\mathbf{x}}_l + 0 \hat{\mathbf{y}}_l$. It follows that:

$$\mathbf{F}_A = (v_{ox}^l + v_{px}^l) \hat{\mathbf{x}}_l + v_{oy}^l \hat{\mathbf{y}}_l,$$

$$\mathbf{F}_B = (v_{ox}^l + v_{px}^l) \hat{\mathbf{x}}_l - v_{oy}^l \hat{\mathbf{y}}_l,$$

i.e., that the vector \mathbf{F}_B is a reflection of vector \mathbf{F}_A about the line l . This completes the proof. ■

Remark 2: The Jacobian matrix of \mathbf{F} is singular at $\mathbf{r} = \mathbf{0}$, which implies that $\mathbf{r} = \mathbf{0}$ is a high-order singularity. Thus, one may expect that the pattern of the integral curves around the singular point will be more complicated compared to those around a first-order singularity, i.e., around nodes, saddles, foci or centers.

Theorem 3: The equation of the integral curves of \mathbf{F} for $\mathbf{p} = [1 \ 0]^T$ is given as:

$$(x^2 + y^2)^{\frac{\lambda}{2}} = c y^{(\lambda-1)}, \quad c \in \mathbb{R}. \quad (9)$$

Proof: Consider the polar coordinates $(r \cos \phi, r \sin \phi)$ of a point (x, y) where:

$$r = \sqrt{x^2 + y^2}, \quad \cos \phi = \frac{x}{r}, \quad \sin \phi = \frac{y}{r}. \quad (10)$$

After substituting (10) and $p_x = 1, p_y = 0$ into (4) the vector field components read:

$$F_x = r^2 ((\lambda - 1) \cos^2 \phi - \sin^2 \phi), \quad (11a)$$

$$F_y = r^2 (\lambda \cos \phi \sin \phi). \quad (11b)$$

An integral curve of (1) is by definition the solution of the system of ordinary differential equations:

$$\begin{aligned} \frac{dx}{dt} &= F_x, \\ \frac{dy}{dt} &= F_y, \end{aligned} \quad \text{which further reads:} \quad \frac{dx}{dy} = \frac{F_x}{F_y}, \quad (12)$$

while the differentials between Cartesian and polar coordinates satisfy the formula:

$$\begin{bmatrix} dr \\ r d\phi \end{bmatrix} = \begin{bmatrix} \cos \phi & \sin \phi \\ -\sin \phi & \cos \phi \end{bmatrix} \begin{bmatrix} dx \\ dy \end{bmatrix}. \quad (13)$$

Plugging (13), (11) into (12) results in:

$$\frac{1}{r} dr = (\lambda - 1) \frac{\cos \phi}{\sin \phi} d\phi,$$

while integrating by parts yields:

$$\ln(r) = (\lambda - 1) \ln(\sin \phi) + \ln(c) \Rightarrow$$

$$\ln(r) = \ln(c \sin^{(\lambda-1)} \phi) \Rightarrow$$

$$r = c \sin^{(\lambda-1)} \phi \Rightarrow r = c \frac{y^{(\lambda-1)}}{r^{(\lambda-1)}} \Rightarrow$$

$$r^\lambda = c y^{(\lambda-1)} \Rightarrow (x^2 + y^2)^{\frac{\lambda}{2}} = c y^{(\lambda-1)}, \quad \text{where } c \in \mathbb{R}.$$

This completes the proof. ■

Remark 3: It is straightforward to verify that:

- For $\lambda = 0$, (9) reduces to $y = c$, i.e., the integral curves are straight lines parallel to $\mathbf{p} = [1 \ 0]^T$.
- For $\lambda = 1$, (9) reduces to $\sqrt{x^2 + y^2} = c$, i.e., the integral curves are circles of radius \sqrt{c} , where $c > 0$, centered at the origin $(x, y) = (0, 0)$.

B. Attractive vector fields

Let us consider the case $\lambda = 2$. Take for simplicity $\mathbf{p} = [1 \ 0]^T$ and write the vector field components as:

$$F_x = x^2 - y^2, \quad (14a)$$

$$F_y = 2xy \quad (14b)$$

Following [34], the singular point $\mathbf{r} = \mathbf{0}$ of (14) is a dipole. More specifically, the vector field (14) has two elliptic sectors, with the axis $y = 0$ serving as the separatrix. This implies that all integral curves *begin and end at the singular point, except for the separatrix $y = 0$* . The separatrix converges to $\mathbf{r} = \mathbf{0}$ for $x < 0$ and diverges for $x > 0$ (Fig. 3). Out of Theorem 2, the separatrix $y = 0$ is the reflection line for the vector field (14).

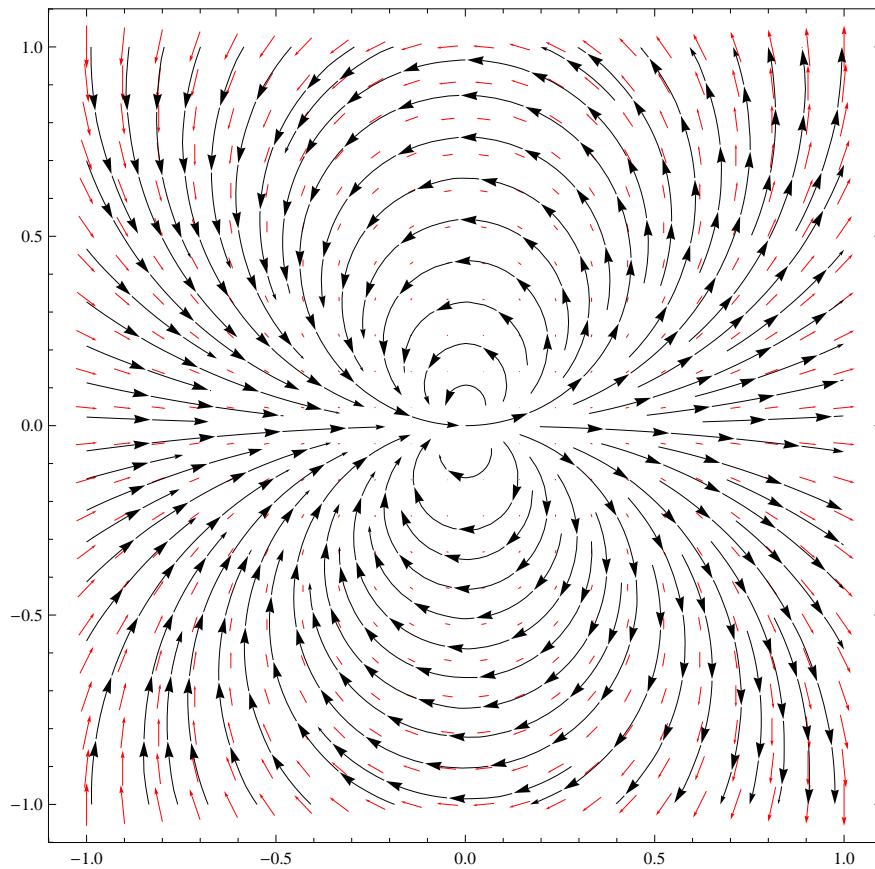


Fig. 3. The integral curves of (1) for $\lambda = 2$, $p_x = 1$, $p_y = 0$.

Furthermore, Theorem 2 implies that the axis the vector $\mathbf{p} \neq \mathbf{0}$ lies on is, in general, a

reflection line for (1). This means that the resulting integral curves are symmetric w.r.t. the vector $\mathbf{p} \in \mathbb{R}^2$. In that sense, any of the integral curves of \mathbf{F} offers a path to $\mathbf{r} = \mathbf{0}$, while at the same time the direction of the vector \mathbf{p} dictates the symmetry axis of the integral curves w.r.t. the global frame \mathcal{G} .

Therefore, defining a feedback motion plan for steering the unicycle to a goal configuration $\mathbf{q}_g = [\mathbf{r}_g^T \ \theta_g]^T$ has been based in earlier work of ours' [33] on the following simple idea: Pick a vector field \mathbf{F} out of (1) in terms of $(\mathbf{r} - \mathbf{r}_g)^2$ with $\lambda = 2$ and $\mathbf{p} = [p_x \ p_y]^T$, so that the direction of the vector \mathbf{p} coincides with the goal orientation: $\varphi \triangleq \arctan(\frac{p_y}{p_x}) = \theta_g$. Then, the integral curves serve as a reference to steer the position trajectories $\mathbf{r}(t)$ to the goal position \mathbf{r}_g , and the orientation trajectories $\theta(t)$ to the goal orientation θ_g .

C. Repulsive vector fields

Let us consider the case $\lambda = 1$, i.e., the case when the vector field (1) has multiple singular points. The vector field components read:

$$F_x = p_y xy - p_x y^2, \quad (15a)$$

$$F_y = p_x xy - p_y x^2. \quad (15b)$$

The vector field (15) vanishes on the set $\mathcal{V} = \{\mathbf{r} \in \mathbb{R}^2 \mid p_y x - p_x y = 0\}$. Out of Theorem 2, the singularity set \mathcal{V} coincides with the reflection line of the vector field (15). The equation of the integral curves can be computed for $p_y x - p_x y \neq 0$ as: $\frac{dx}{dy} = \frac{y}{-x} \Rightarrow x^2 + y^2 = c^2$, where $c \in \mathbb{R}$, which implies that the integral curves are circles centered at the origin $\mathbf{r} = \mathbf{0}$, see Fig. 4.

The signum of x (in general, of $\mathbf{p}_i^T \mathbf{r}$) dictates whether the integral curves escape the singularity set \mathcal{V} (see the half-plane $x > 0$) or converge to the singularity set \mathcal{V} (see the half-plane $x < 0$). We say that the singular point $\mathbf{r} = \mathbf{0}$ of the vector field (15) is of center type; this means that *no integral curve reaches the singular point.*³

Thus, one may employ (15) to define tangential vector fields locally around circular obstacles.

²This is to have the unique singular point of \mathbf{F} coinciding with the desired position \mathbf{r}_g .

³Characterizing this particular singularity as of center type is slightly inconsistent with standard notation, since in this case the singular point $\mathbf{r} = \mathbf{0}$ is not isolated.

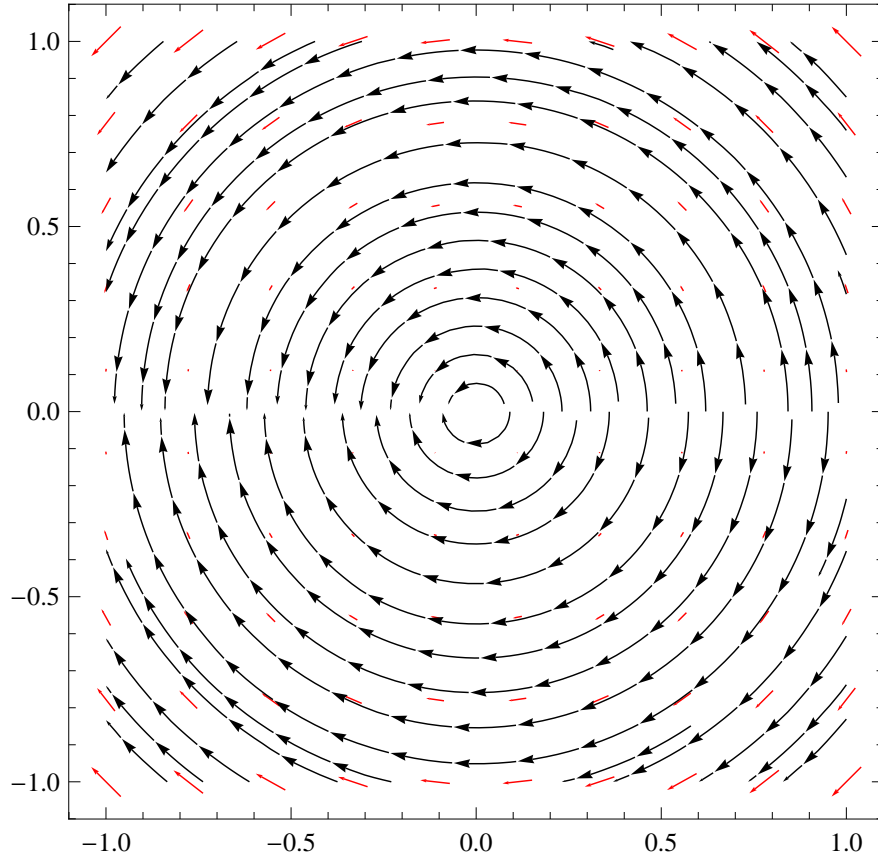


Fig. 4. The vector field \mathbf{F} for $\lambda = 1$ and $p_x = 1, p_y = 0$.

IV. ALMOST GLOBAL FEEDBACK MOTION PLANS

Given the class of attractive and repulsive vector fields, the idea on defining an almost global feedback motion plan \mathbf{F}^* on the collision-free space \mathcal{F} is now simple: we pursue to combine an attractive-to-the-goal vector field \mathbf{F}_g with (local) repulsive vector fields \mathbf{F}_{oi} around each obstacle \mathcal{O}_i , so that the integral curves of \mathbf{F}^* : 1) converge to the goal \mathbf{q}_g , and 2) point into the interior of \mathcal{F} on the boundaries of the obstacles \mathcal{O}_i . The vector field \mathbf{F}^* can then serve as a feedback motion plan on \mathcal{W} .

Remark 4: Combining the vector fields $\mathbf{F}_g, \mathbf{F}_{oi}$ should be done carefully so that the resulting vector field \mathbf{F}^* does not have any undesired singularities on \mathcal{F} . For this reason, we consider the

normalized unit vector fields:

$$\mathbf{F}_g^n = \begin{cases} \frac{\mathbf{F}_g}{\|\mathbf{F}_g\|}, & \text{for } \mathbf{r} \neq \mathbf{0}; \\ \mathbf{0}, & \text{for } \mathbf{r} = \mathbf{0}. \end{cases} \quad (16a)$$

$$\mathbf{F}_{oi}^n = \begin{cases} \frac{\mathbf{F}_{oi}}{\|\mathbf{F}_{oi}\|}, & \text{for } \mathbf{r} \notin \mathcal{V}_i; \\ \mathbf{0}, & \text{for } \mathbf{r} \in \mathcal{V}_i. \end{cases} \quad (16b)$$

respectively, when defining the blending mechanism, see later on in Section IV-C.

A. Attractive vector field to the goal

Without loss of generality we assume that $\mathbf{q}_g = \mathbf{0}$. An attractive-to-the-goal vector field \mathbf{F}_g may be taken out of (1) for $\lambda = 2$, $\mathbf{p}_g = [1 \ 0]^T$, which yields the vector field (14). The components of the normalized vector field \mathbf{F}_g^n taken out of (16a) for $x \neq 0$, $y \neq 0$ read:

$$F_{gx}^n = \frac{x^2 - y^2}{x^2 + y^2}, \quad F_{gy}^n = \frac{2xy}{x^2 + y^2}.$$

B. Repulsive vector field w.r.t. a circular obstacle

Consider an obstacle \mathcal{O}_i and the region $\mathcal{Z}_i : \{\mathbf{r} \in \mathbb{R}^2 \mid \|\mathbf{r} - \mathbf{r}_{oi}\| \leq \varrho_{\mathcal{Z}_i}\}$, where $\varrho_{\mathcal{Z}_i} = \varrho_{oi} + \varrho + \varrho_\varepsilon$, see Fig. 5. The parameter $\varrho_\varepsilon \geq 0$ is the minimum distance that the robot is allowed to keep w.r.t. the boundary of the obstacle.

A repulsive vector field w.r.t. the point \mathbf{r}_{oi} can be picked out of (15) for $\mathbf{p}_i = [p_{xi} \ p_{yi}]^T$, where $p_{xi} = \cos \phi_i$, $p_{yi} = \sin \phi_i$, $\phi_i = \text{atan2}(-y_{oi}, -x_{oi}) + \pi$ as:

$$F_{oxi} = p_{yi}(x - x_{oi})(y - y_{oi}) - p_{xi}(y - y_{oi})^2, \quad (17a)$$

$$F_{oyi} = p_{xi}(x - x_{oi})(y - y_{oi}) - p_{yi}(x - x_{oi})^2. \quad (17b)$$

Note that the vector \mathbf{p}_i is picked such that it lies on the line connecting the center \mathbf{r}_{oi} of the obstacle with the goal point $\mathbf{r}_g = \mathbf{0}$. Therefore, the singularity set \mathcal{V}_i of (17) lies by construction on this line, which is also the reflection axis of the vector field (17). Denote $\mathcal{A}_i = \{\mathbf{r} \in \mathcal{Z}_i \mid \mathbf{p}_i^T(\mathbf{r} - \mathbf{r}_{oi}) \geq 0\}$, $\mathcal{B}_i = \{\mathbf{r} \in \mathcal{Z}_i \mid \mathbf{p}_i^T(\mathbf{r} - \mathbf{r}_{oi}) < 0\}$, where $\mathcal{Z}_i = \mathcal{A}_i \cup \mathcal{B}_i$, and consider the behavior of the integral curves around the singularity set \mathcal{V}_i . The integral curves depart from the singularity set \mathcal{V}_i in the region \mathcal{A}_i (see the red vectors around \mathcal{V}_i in Fig. 5), and converge to the singularity set \mathcal{V}_i in the region \mathcal{B}_i (the corresponding vectors have *not* been drawn in Fig. 5). The integral curves in region \mathcal{A}_i render safe, tangential reference paths around the obstacle

In summary, the vector field \mathbf{F}_{oi} around a circular obstacle \mathcal{O}_i is picked out of the family of vector fields (1) as:

$$\mathbf{F}_{oi} = \begin{cases} \mathbf{F}_{(\lambda=1)}(\delta\mathbf{r}_i), & \text{for } \mathbf{p}_i^T(\delta\mathbf{r}_i) \geq 0; \\ \mathbf{F}_{(\lambda=0)}(\delta\mathbf{r}_i), & \text{for } \mathbf{p}_i^T(\delta\mathbf{r}_i) < 0, \end{cases} \quad (19)$$

where $\delta\mathbf{r}_i \triangleq \mathbf{r} - \mathbf{r}_{oi}$, $\phi_i \triangleq \text{atan2}(-y_{oi}, -x_{oi}) + \pi$, $\mathbf{p}_i = [\cos \phi_i \quad \sin \phi_i]^T$. The normalized vector field then reads:

$$\mathbf{F}_{oi}^n = \begin{cases} \frac{\mathbf{F}_{(\lambda=0)}(\delta\mathbf{r}_i)}{\|\mathbf{F}_{(\lambda=0)}(\delta\mathbf{r}_i)\|}, & \text{for } \mathbf{p}_i^T(\delta\mathbf{r}_i) < 0; \\ \frac{\mathbf{F}_{(\lambda=1)}(\delta\mathbf{r}_i)}{\|\mathbf{F}_{(\lambda=1)}(\delta\mathbf{r}_i)\|}, & \text{for } \mathbf{p}_i^T(\delta\mathbf{r}_i) \geq 0 \text{ and } \mathbf{r} \notin \mathcal{V}_i; \\ \mathbf{0}, & \text{for } \mathbf{p}_i^T(\delta\mathbf{r}_i) \geq 0 \text{ and } \mathbf{r} \in \mathcal{V}_i; \end{cases} \quad (20)$$

C. Blending attractive and repulsive vector fields

Define the obstacle function $\beta_i(\cdot) : \mathbb{R}^2 \rightarrow \mathbb{R}$ as:

$$\beta_i(\mathbf{r}, \mathbf{r}_{oi}, \varrho_{oi}) = \varrho_{oi}^2 - \|\mathbf{r} - \mathbf{r}_{oi}\|^2, \quad (21)$$

which is positive in the interior $\text{Int}(\mathcal{O}_i)$ of the obstacle, zero on the boundary $\partial\mathcal{O}_i$ of the obstacle, and negative everywhere else. Denote the value of the constraint function β_i on the boundary $\partial\mathcal{Z}_i$ of the region \mathcal{Z}_i as $\beta_{i\mathcal{Z}} = -2\varrho_{oi}(\varrho + \varrho_\varepsilon) - (\varrho + \varrho_\varepsilon)^2$.

The repulsive vector field \mathbf{F}_{oi}^n is then locally defined on the set: $(\mathcal{Z}_i \setminus \text{Int}(\mathcal{O}_i)) = \{\mathbf{r} \in \mathbb{R}^2 \mid \beta_{i\mathcal{Z}} \leq \beta_i(\mathbf{r}) \leq 0\}$. At the same time, the attractive vector field \mathbf{F}_g^n should be defined exterior to \mathcal{Z}_i , i.e., for $\beta_i(\mathbf{r}) < \beta_{i\mathcal{Z}}$. To encode this, define the smooth bump function $\sigma_i(\cdot) : \mathbb{R}^2 \rightarrow [0, 1]$:

$$\sigma_i = \begin{cases} 1, & \text{for } \beta_i(\mathbf{r}) \leq \beta_{i\mathcal{F}}; \\ a\beta_i^3 + b\beta_i^2 + c\beta_i + d, & \text{for } \beta_{i\mathcal{F}} < \beta_i(\mathbf{r}) < \beta_{i\mathcal{Z}}; \\ 0, & \text{for } \beta_{i\mathcal{Z}} \leq \beta_i(\mathbf{r}); \end{cases} \quad (22)$$

where $\beta_{i\mathcal{Z}}$ is the value of (21) at distance $\varrho_{\mathcal{Z}i}$ w.r.t. \mathbf{r}_{oi} , $\beta_{i\mathcal{F}}$ is the value of (21) at some distance $\varrho_{\mathcal{F}i} > \varrho_{\mathcal{Z}i}$ w.r.t. \mathbf{r}_{oi} , and the coefficients a , b , c and d are computed as:

$$a = \frac{2}{(\beta_{i\mathcal{Z}} - \beta_{i\mathcal{F}})^3}, \quad b = -\frac{3(\beta_{i\mathcal{Z}} + \beta_{i\mathcal{F}})}{(\beta_{i\mathcal{Z}} - \beta_{i\mathcal{F}})^3},$$

$$c = \frac{6\beta_{i\mathcal{Z}}\beta_{i\mathcal{F}}}{(\beta_{i\mathcal{Z}} - \beta_{i\mathcal{F}})^3}, \quad d = \frac{\beta_{i\mathcal{Z}}^2(\beta_{i\mathcal{Z}} - 3\beta_{i\mathcal{F}})}{(\beta_{i\mathcal{Z}} - \beta_{i\mathcal{F}})^3},$$

so that (22) is a \mathcal{C}^2 function. Having this at hand, and inspired by [17], one may now define the vector field:

$$\mathbf{F}_i = \sigma_i \mathbf{F}_g^n + (1 - \sigma_i) \mathbf{F}_{oi}^n. \quad (23)$$

Lemma 1: The vector field (23) is:

- (i) Attractive to the goal \mathbf{q}_g for $\|\mathbf{r} - \mathbf{r}_{oi}\| \geq \varrho_{\mathcal{F}_i}$, i.e., for $\beta_i(\mathbf{r}) \leq \beta_{\mathcal{F}_i}$ where $\sigma_i = 1$, via the effect of \mathbf{F}_g^n .
- (ii) Repulsive w.r.t. \mathcal{O}_i for $\varrho_{oi} \leq \|\mathbf{r} - \mathbf{r}_{oi}\| \leq \varrho_{\mathcal{Z}_i}$, i.e., for $\beta_{\mathcal{Z}_i} \leq \beta_i(\mathbf{r})$ where $\sigma_i = 0$, via the effect of \mathbf{F}_{oi}^n .
- (iii) Nonsingular in the region $\varrho_{\mathcal{Z}_i} < \|\mathbf{r} - \mathbf{r}_{oi}\| < \varrho_{\mathcal{F}_i}$, i.e., for $\beta_{\mathcal{F}_i} < \beta_i(\mathbf{r}) < \beta_{\mathcal{Z}_i}$ where $0 < \sigma_i < 1$.
- (iv) Safe w.r.t. the obstacle \mathcal{O}_i and convergent to the goal \mathbf{q}_g for almost all initial conditions.

Proof: The first two arguments have been proved in the previous section. To verify the third argument, consider the norm of vector field \mathbf{F}_i in the blending region $\mathcal{D}_i : \{\mathbf{r} \in \mathbb{R}^2 \mid \varrho_{\mathcal{Z}_i} < \|\mathbf{r} - \mathbf{r}_{oi}\| < \varrho_{\mathcal{F}_i}\}$, which reads:

$$\|\mathbf{F}_i\| = \sqrt{1 - 2\sigma_i(1 - \sigma_i) + 2\sigma_i(1 - \sigma_i) \cos \alpha},$$

where α the angle between the vectors \mathbf{F}_g^n , \mathbf{F}_{oi}^n at some point $\mathbf{r} \in \mathcal{D}_i$. Then, for $\mathbf{r} \notin \mathcal{V}_i$ one has that $\|\mathbf{F}_i\|$ vanishes at the points where σ_i is the solution of:

$$2(1 - \cos \alpha)\sigma_i^2 - 2(1 - \cos \alpha)\sigma_i + 1 = 0.$$

The discriminant reads $\Delta = -4(1 - \cos \alpha)^2$, which implies that there are no real solutions, i.e., that the vector field \mathbf{F}_i is nonsingular for $\mathbf{r} \notin \mathcal{V}_i$. Moreover, for $\mathbf{r} \in \mathcal{V}_i$ one has $\mathbf{F}_{oi}^n = \mathbf{0}$, and therefore: $\|\mathbf{F}_i\| = \sigma_i \neq 0$.

Finally, to verify the fourth argument, consider first that the integral curves which do not intersect with the blending region \mathcal{D}_i are convergent by construction to \mathbf{r}_g . Consider now the boundary

$$S_i : \{\mathbf{r} \in \mathbb{R}^2 \mid \|\mathbf{r} - \mathbf{r}_{oi}\|^2 - \varrho_{\mathcal{F}_i}^2 = 0\}$$

of the region \mathcal{D}_i and let us analyze the behavior of the integral curves on the manifolds:

$$S_i^- : \{\mathbf{r} \in \mathbb{R}^2 \mid \|\mathbf{r} - \mathbf{r}_{oi}\| = \varrho_{\mathcal{F}_i} + \delta\varrho\},$$

$$S_i^+ : \{\mathbf{r} \in \mathbb{R}^2 \mid \|\mathbf{r} - \mathbf{r}_{oi}\| = \varrho_{\mathcal{F}_i} - \delta\varrho\},$$

with $\delta\rho > 0$ arbitrarily small. After some calculations:

$$\nabla S_i \mathbf{F}_i = 2(\mathbf{r} - \mathbf{r}_{oi})^T \mathbf{F}_g^n,$$

$$\nabla S_i^- \mathbf{F}_i = 2(\mathbf{r} - \mathbf{r}_{oi})^T \mathbf{F}_g^n.$$

For $\nabla S_i^+ \mathbf{F}_i$, consider the following cases:

Case 1. The vector field \mathbf{F}_{oi}^n satisfies: $(\mathbf{r} - \mathbf{r}_{oi})^T \mathbf{F}_{oi}^n = 0$, and therefore:

$$\nabla S_i^+ \mathbf{F}_i = 2\sigma_i(\mathbf{r} - \mathbf{r}_{oi})^T \mathbf{F}_g^n.$$

Then: $(\nabla S_i^- \mathbf{F}_i)(\nabla S_i^+ \mathbf{F}_i) > 0$, which implies that the integral curves cross the switching surface S_i and enter \mathcal{A}_i . Consider now the behavior of the integral curves in \mathcal{A}_i . Assume that $\nabla S_i^+ \mathbf{F}_i = 2\sigma_i(\mathbf{r} - \mathbf{r}_{oi})^T \mathbf{F}_g^n > 0$; this would imply that $\nabla S_i \mathbf{F}_i > 0$ as well, i.e., that the integral curves did not cross S_i , a contradiction. Then:

$$\nabla S_i^+ \mathbf{F}_i = 2\sigma_i(\mathbf{r} - \mathbf{r}_{oi})^T \mathbf{F}_g^n < 0,$$

which yields that the integral curves approach the boundary

$$T_i : \{\mathbf{r} \in \mathbb{R}^2 \mid \|\mathbf{r} - \mathbf{r}_{oi}\|^2 - \varrho_{Zi}^2 = 0\}$$

of the blending region \mathcal{D}_i . Denote

$$T_i^- : \{\mathbf{r} \in \mathbb{R}^2 \mid \|\mathbf{r} - \mathbf{r}_{oi}\| = \varrho_{Zi} + \delta\rho\}$$

and note that: $\nabla T_i^- \mathbf{F}_i = \nabla S_i^+ \mathbf{F}_i < 0$, and that $\nabla T_i \mathbf{F}_i = 0$, since on T_i one has $\sigma_i = 0$. Then, $\mathbf{F}_i \neq \mathbf{0}$ is tangent to T_i , which means that the integral curves slide along T_i , until reaching region \mathcal{B}_i .

Remark 6: The integral curves are not defined on the (unique) point on T_i where $\mathbf{F}_i = \mathbf{0}$. This further implies that system trajectories which either start or reach this point get stuck away from the goal configuration.

Let us now consider the pattern of the integral curves in the vicinity of the singularity and characterize the set of initial conditions from which the system trajectories end there. It was shown in the previous section that the integral curves around the singularity set \mathcal{V}_i are departing the set, except for one integral curve which converges to \mathcal{V}_i . For this condition to occur *the goal orientation θ_g should be co-linear with the line the singularity set \mathcal{V}_i lies on.*

To see why, recall that the vector field in the blending region reads: $\mathbf{F}_i = \sigma_i \mathbf{F}_g^n$, and that

the vector field \mathbf{F}_g^n should point to the singularity set \mathcal{V}_i . Consequently, this condition arises if and only if the obstacle is positioned such that the direction of the vector \mathbf{p}_i coincides with the direction of the vector \mathbf{p}_g . Therefore, the set of initial conditions from which the integral curves of \mathbf{F}_i converge to the singularity set \mathcal{V}_i is of Lebesgue measure zero. Note also that if the direction of \mathbf{p}_g does not coincide with the direction of \mathbf{p}_i , then the singular points of \mathbf{F}_i are confined in \mathcal{Z}_i on a line segment of length ϱ_ε , correspond to the initial conditions from which solutions are not defined, and are reached by no integral curve.

Case 2. In region \mathcal{B}_i one may follow a similar analysis to conclude that the integral curves exit \mathcal{B}_i .

In summary, the vector field (23) is safe and globally convergent almost everywhere, i.e., except for a set of initial conditions of measure zero. \blacksquare

D. Motion plan in static obstacle environments

Theorem 4: Assume a workspace \mathcal{W} of N circular obstacles \mathcal{O}_i , $i \in \{1, \dots, N\}$, positioned such that the inter-obstacle distances $d_{ij} = \|\mathbf{r}_{oi} - \mathbf{r}_{oj}\|$ satisfy:

$$d_{ij} \geq \varrho_{z_i} + \varrho_{z_j}, \forall (i, j), j \in \{1, \dots, N\}, j \neq i. \quad (24)$$

Then, the vector field $\mathbf{F}^* : \mathbb{R}^2 \rightarrow \mathbb{R}^2$, given as:

$$\mathbf{F}^* = \prod_{i=1}^N \sigma_i \mathbf{F}_g + \sum_{i=1}^N (1 - \sigma_i) \mathbf{F}_{oi}, \quad (25)$$

where \mathbf{F}_g is the normalized attractive vector field (16a), \mathbf{F}_{oi} is the normalized repulsive vector field (20) around an obstacle \mathcal{O}_i , and σ_i is the bump function (22) defined in terms of the obstacle function β_i given by (21), is a safe, almost global feedback motion plan in \mathcal{F} , except for a set of initial conditions of measure zero.

Proof: By construction, the first term in (25) cancels the effect of the attractive vector field \mathbf{F}_g where at least one of the bump functions $\sigma_i = 0$, i.e., in the corresponding region \mathcal{Z}_i around obstacle \mathcal{O}_i . At the same time the second term shapes the corresponding vector field \mathbf{F}_{oi} in \mathcal{Z}_i . Thus, the attractive vector field \mathbf{F}_g is activated through (25) only when $\beta_i < \beta_{z_i} \forall i \in \{1, \dots, N\}$, i.e., outside the regions \mathcal{Z}_i . Furthermore, setting the inter-obstacle distance $d_{ij} \geq \varrho_{z_i} + \varrho_{z_j}$ implies that the repulsive flows around obstacles do not overlap, and therefore

are both safe and almost globally convergent to the goal, as proved in Lemma 1. This completes the proof. \blacksquare

Remark 7: The condition (24) reads that the minimum distance among the boundaries of the obstacles should be at least $2(\varrho + \varrho_\varepsilon)$. This clearance is not conservative or restrictive in practice, since the parameter ϱ_ε can be chosen arbitrarily close to zero, or even equal to zero, in case the robot is allowed to touch the obstacle.

E. Control design and simulation results

Having (25) at hand, the control design for the unicycle (2) is now straightforward. We use the control law:

$$u = k_u \tanh(\|\mathbf{r} - \mathbf{r}_g\|^2), \quad (26a)$$

$$\omega = -k_\omega(\theta - \varphi) + \dot{\varphi}, \quad (26b)$$

where $\varphi \triangleq \arctan\left(\frac{F_y^*}{F_x^*}\right)$ is the orientation of the vector field \mathbf{F}^* at a point (x, y) , with its time derivative reading:

$$\dot{\varphi} \stackrel{(2)}{=} \left(\left(\frac{\partial F_y^*}{\partial x} c\theta + \frac{\partial F_y^*}{\partial y} s\theta \right) F_x^* - \left(\frac{\partial F_x^*}{\partial x} c\theta + \frac{\partial F_x^*}{\partial y} s\theta \right) F_y^* \right) u,$$

with the linear velocity u given by (26a), see in [35], and $k_\omega > 0$, $k_u > 0$. Then, the orientation θ of the unicycle is Globally Exponentially Stable (GES) to the safe orientation φ , and the robot flows along the integral curves of \mathbf{F}^* until converging to \mathbf{r}_g .

To demonstrate the efficacy of the proposed navigation and control design we consider the motion of a robot in an environment with $N = 10$ static obstacles (Fig. 6), where the goal position is $\mathbf{r}_g = [-0.1 \ 0.08]^T$. The radii of the obstacles are set equal to $\varrho_{oi} = 0.03$. The blending zone \mathcal{D}_i around each obstacle \mathcal{O}_i is illustrated between the boundary surfaces S_i (black line) and T_i (red line), respectively. The resulting collision-free path under the control law (26), with the control gains picked equal to $k_u = 0.075$, $k_r = 2.5$, are depicted in blue color.

Remark 8: The integral curves of \mathbf{F}_{oi} in the region \mathcal{A}_i around an obstacle \mathcal{O}_i forces the robot to perform a sharp maneuver in order to follow the tangential direction and avoid collision. This in practice is plausible for unicycle-type vehicles (e.g. differentially driven mobile robots), yet it may not be desirable for input-constrained vehicles, such as car-like vehicles and aircraft. Our current work focuses in encoding curvature constraints via (1).

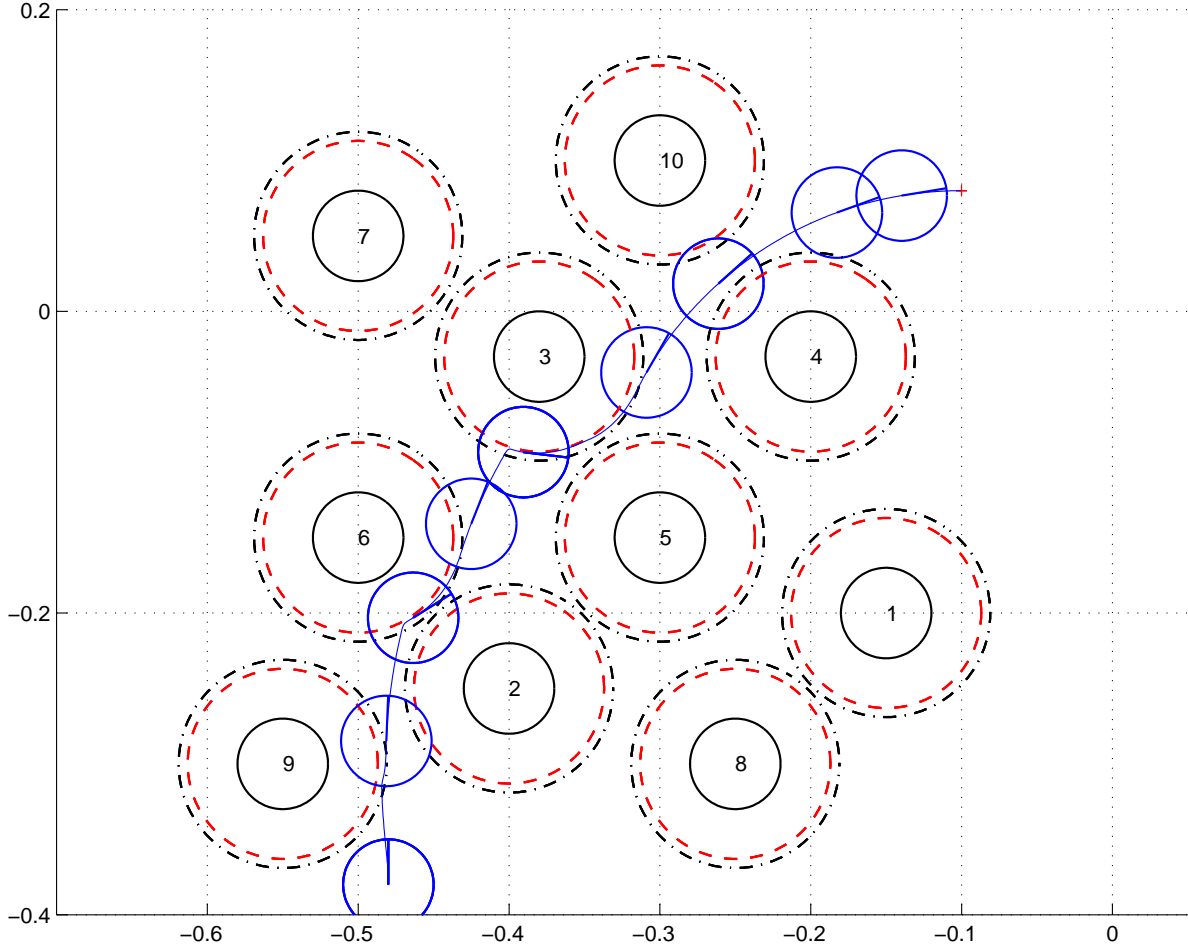


Fig. 6. The path of a unicycle in an obstacle environment.

V. EXTENSION TO DYNAMIC ENVIRONMENTS

Consider N agents $i \in \{1, 2, \dots, N\}$ of unicycle kinematics which are assigned with the task to converge to goal configurations \mathbf{q}_{gi} while avoiding collisions.

Each agent i has a circular communication/sensing region \mathcal{C}_i of radius R_c centered at $\mathbf{r}_i = \begin{bmatrix} x_i & y_i \end{bmatrix}^T$, denoted as:

$$\mathcal{C}_i : \{\mathbf{r} \in \mathbb{R}^2 \mid \|\mathbf{r}_i - \mathbf{r}\| \leq R_c\},$$

and can reliably exchange information with any agent $j \neq i$ which lies within its communication region \mathcal{C}_i . In other words, we say that a pair of agents (i, j) is connected, or equivalently, that agent j is neighbor to agent i , as long as the inter-agent distance $d_{ij} = \|\mathbf{r}_i - \mathbf{r}_j\| \leq R_c$. Denote the set of neighbors $j \neq i$ of agent i with \mathcal{N}_i .

Agents $j \neq i$ serve as dynamic (moving) obstacles to agent i . Navigating safely to an assigned goal \mathbf{q}_{gi} is then reduced into finding a feedback motion plan \mathbf{F}_i^* such that its integral curves: (i) point into the interior of the collision-free space \mathcal{F}_i on the boundaries of the agents $j \neq i$, and (ii) converge to the goal \mathbf{q}_{gi} . Towards this end, we would like to employ a vector field \mathbf{F}_i^* for each agent i as:

$$\mathbf{F}_i^* = \prod_{j \in \mathcal{N}_i} \sigma_{ij} \mathbf{F}_{gi} + \sum_{j \in \mathcal{N}_i} (1 - \sigma_{ij}) \mathbf{F}_{oj}^i, \quad (27)$$

where the attractive term \mathbf{F}_{gi} is taken out of (16a), the bump function σ_{ij} is defined later on, and the repulsive term \mathbf{F}_{oj}^i around each agent $j \neq i$ is replaced with a normalized repelling node,⁴ given out of:

$$\mathbf{F}_{xoj}^i = \frac{x_i - x_j}{\sqrt{(x_i - x_j)^2 + (y_i - y_j)^2}}, \quad (28a)$$

$$\mathbf{F}_{yoj}^i = \frac{y_i - y_j}{\sqrt{(x_i - x_j)^2 + (y_i - y_j)^2}}. \quad (28b)$$

In order to utilize the (almost global) convergence and safety guarantees applying to the static case, we need to ensure that the repulsive flows around agents do not overlap, for any pair of agents (i, j) . Recall from the static case that this condition equivalently reads as that the minimum distance d_m between any pair of (moving, in the dynamic case) agents (i, j) is $d_m = 2(2\varrho + \varrho_\epsilon)$, or equivalently, that the minimum clearance between any pair of agents is $(2\varrho + \varrho_\epsilon)$, where $\varrho_\epsilon > 0$ arbitrarily small and ϱ is the radius of the agents.

In that respect, the bump function σ_{ij} in (27) is defined as:

$$\sigma_{ij} = \begin{cases} 1, & \text{for } d_m \leq d_{ij} \leq d_r; \\ a d_{ij}^3 + b d_{ij}^2 + c d_{ij} + d, & \text{for } d_r < d_{ij} < d_c; \\ 0, & \text{for } d_{ij} \geq d_c; \end{cases} \quad (29)$$

where the coefficients a, b, c, d have been computed as:

$$\begin{aligned} a &= -\frac{2}{(d_r - d_c)^3}, & b &= \frac{3(d_r + d_c)}{(d_r - d_c)^3}, \\ c &= -\frac{6 d_r d_c}{(d_r - d_c)^3}, & d &= \frac{d_c^2(3d_c - d_r)}{(d_r - d_c)^3}, \end{aligned}$$

⁴The tangential repulsive vector field (19) defined for static obstacles is not a suitable choice for the dynamic case; the reason is that the repulsive integral curves of the vector field (25) of agent i around agent j are rendered an invariant set under the proposed velocity coordination protocol, forcing thus the trajectories $\mathbf{r}_i(t), \mathbf{r}_j(t)$ of a pair of agents i, j converge to undesired locations away from the goal locations $\mathbf{r}_{gi}, \mathbf{r}_{gj}$, see also the analysis in [?].

so that (22) is a \mathcal{C}^2 function, $d_m \geq 2(2\varrho + \varrho_\epsilon)$, $d_m < d_r < d_c$.

Remark 9: The communication/sensing range of each agent i should be $R_c \geq d_c$.

A. Control design

Each agent i moves under the control law:

$$u_i = \begin{cases} \max \left\{ 0, \min_{j \in \mathcal{N}_i | J_j < 0} u_{i|j} \right\}, & d_m \leq d_{ij} \leq R_c, \\ u_{ic}, & R_c < d_{ij}; \end{cases}, \quad (30a)$$

$$\omega_i = -k_{\omega i} (\theta_i - \varphi_i) + \dot{\varphi}_i, \quad (30b)$$

where: φ_i is the orientation of the vector field \mathbf{F}_i^* at a point (x, y) , the vector field \mathbf{F}_i^* is given by (27), $u_{i|j}$ is the safe velocity of agent i w.r.t. an agent j lying in the communication region of \mathcal{C}_i of agent i , given as:

$$u_{i|j} = u_{ic} \frac{d_{ij} - d_m}{R_c - d_m} + \varepsilon_i u_{is|j} \frac{R_c - d_{ij}}{R_c - d_m}, \quad (31)$$

with the terms in (31) defined as:

$$u_{ic} = k_{ui} \tanh(\|\mathbf{r}_i - \mathbf{r}_{gi}\|), \quad u_{is|j} = u_j \frac{\mathbf{r}_{ji}^T \boldsymbol{\eta}_j}{\mathbf{r}_{ji}^T \boldsymbol{\eta}_i},$$

$$\boldsymbol{\eta}_i = \begin{bmatrix} \cos \varphi_i \\ \sin \varphi_i \end{bmatrix}, \quad J_j = \mathbf{r}_{ji}^T \boldsymbol{\eta}_i, \quad \mathbf{r}_{ji} = \mathbf{r}_i - \mathbf{r}_j,$$

and $\varepsilon_i > 1$, $k_{ui}, k_{\omega i} > 0$.

Theorem 5: Consider N agents $i \in \{1, \dots, N\}$ assigned to converge to goal configurations \mathbf{q}_{gi} . Then, under the control law (30) each agent safely converges to its goal configuration almost globally, except for a set of initial conditions of measure zero.

Proof: The closed loop trajectories of each agent i are forced to flow along the vector field (27). If $d_{ij}(t) > R_c$, $\forall t \geq 0$ and $\forall j \in \{1, \dots, N\}$, then $\sigma_{ij}(t) = 1$, implying that agent i flows safely along (16a) and converges to \mathbf{q}_{gi} .

Let us now assume that at some time $t \geq 0$ the distance $d_{ij}(t)$ between a pair of agents (i, j) is $d_{ij}(t) \leq R_c$. By definition agent i lies in the sensing/communication region of agent j and vice versa, which implies that they exchange information on their current positions $\mathbf{r}_i(t)$, $\mathbf{r}_j(t)$ and

velocities $\boldsymbol{\nu}_i(t)$, $\boldsymbol{\nu}_j(t)$. Consider the blending region $\mathcal{D}_i : \{\boldsymbol{r}_j \in \mathbb{R}^2 \mid d_r < \|\boldsymbol{r}_i - \boldsymbol{r}_j\| < d_c\}$ and the surfaces:

$$S_i(t) : \{\boldsymbol{r}_i(t), \boldsymbol{r}_j(t) \in \mathbb{R}^2 \mid \|\boldsymbol{r}_i(t) - \boldsymbol{r}_j(t)\| - d_c = 0\},$$

$$T_i(t) : \{\boldsymbol{r}_i(t), \boldsymbol{r}_j(t) \in \mathbb{R}^2 \mid \|\boldsymbol{r}_i(t) - \boldsymbol{r}_j(t)\| - d_r = 0\}.$$

Lemma 2: Agent i avoids collision with any of its neighbor agents $j \in \mathcal{N}_i$.

Proof: Collision-free motion is realized as ensuring that $d_{ij}(t) \geq 2\varrho$, $\forall t \geq 0$, for any pair (i, j) . Let us consider the time derivative of inter-agent distance function, which after some calculations reads:

$$\begin{aligned} \frac{d}{dt} d_{ij} &= \frac{(x_i - x_j)(\dot{x}_i - \dot{x}_j)}{d_{ij}} + \frac{(y_i - y_j)(\dot{y}_i - \dot{y}_j)}{d_{ij}} \\ &\stackrel{(2)}{=} \frac{u_i \boldsymbol{r}_{ji}^T \boldsymbol{\eta}_i - u_j \boldsymbol{r}_{ji}^T \boldsymbol{\eta}_j}{d_{ij}}. \end{aligned} \quad (32)$$

The control law (30) renders the value of the time derivative (32) positive when the value of the distance function is $d_{ij} = d_m$, implying thus that the inter-agent distance is forced to increase. Since $d_m > 2\varrho$, this further implies that collisions are avoided. ■

In order to draw conclusions about the convergence of the agents' trajectories to their goal configurations we need to examine the behavior of the integral curves around the switching surfaces $S_i(t)$, $T_i(t)$. With the vector fields \mathbf{F}_i^* , \mathbf{F}_j^* well-defined everywhere in the corresponding blending regions, and the linear velocities u_i , u_j vanishing only at the goal locations \boldsymbol{r}_{gi} , \boldsymbol{r}_{gj} , we are interested in identifying conditions under which the system trajectories $\boldsymbol{r}_i(t)$, $\boldsymbol{r}_j(t)$ are forced to get stuck on $S_i(t)$, or on $T_i(t)$, for infinite amount of time. This can be seen as identifying sufficient conditions of the appearance of (chattering) Zeno behavior, or Zeno points [43]. A sufficient condition on the appearance of Zeno points is given in [44], Theorem 2. Based on this result, we study under which conditions the system (i.e., agents') trajectories converge to a Zeno point. Consider the case with $N = 2$ agents. Denote the dynamics of the k -th agent as $\dot{\boldsymbol{q}}_k = \boldsymbol{f}_k(\boldsymbol{q}_k)$, $k \in \{i, j\}$, $\boldsymbol{q} = [\boldsymbol{q}_i^T \ \boldsymbol{q}_j^T]^T$, $\boldsymbol{r} = [\boldsymbol{r}_i^T \ \boldsymbol{r}_j^T]^T$, and take:

$$\nabla S_i \boldsymbol{f}(\boldsymbol{q}) = 2u_i \boldsymbol{r}_{ij}^T \begin{bmatrix} \cos \theta_i \\ \sin \theta_i \end{bmatrix} - 2u_j \boldsymbol{r}_{ij}^T \begin{bmatrix} \cos \theta_j \\ \sin \theta_j \end{bmatrix}, \quad (33)$$

where $\boldsymbol{r}_{ij} = \boldsymbol{r}_i - \boldsymbol{r}_j$. Note that the control law (30b) renders the orientation θ_k of the k -th agent GES to the orientation φ_k of the vector field \mathbf{F}_k^* . Thus, the unit vector $[\cos \theta_k \ \sin \theta_k]^T$ coincides

with the vector field $\mathbf{F}_k^*(\mathbf{r}_k)$, evaluated at $\mathbf{r}_k \in \mathbb{R}^2$. With this at hand and after some algebraic calculations one has:

$$\begin{aligned}\nabla S_i^- \mathbf{f}(\mathbf{q}) &= \underbrace{2u_i \mathbf{r}_{ij}^T \mathbf{F}_{gi} - 2u_j \mathbf{r}_{ij}^T \mathbf{F}_{gj}}_A, \\ \nabla S_i^+ \mathbf{f}(\mathbf{q}) &= \sigma_{ij} (2u_i \mathbf{r}_{ij}^T \mathbf{F}_{gi} - 2u_j \mathbf{r}_{ij}^T \mathbf{F}_{gj}) \\ &\quad + (1 - \sigma_{ij}) \underbrace{(2u_i \mathbf{r}_{ij}^T \mathbf{F}_{oj}^i - 2u_j \mathbf{r}_{ij}^T \mathbf{F}_{oi}^j)}_B.\end{aligned}$$

The set of Zero points is:

$$Z_i = \{\mathbf{r} \in \mathbb{R}^{2N} \mid \nabla S_i^- \mathbf{f}(\mathbf{q}) = \nabla S_i^+ \mathbf{f}(\mathbf{q}) = 0\},$$

which reads:

$$\begin{aligned}A = \sigma_{ij}A + (1 - \sigma_{ij})B = 0 &\Rightarrow A = B = 0 \Rightarrow \\ u_i \mathbf{r}_{ij}^T (\mathbf{F}_{gi} - \mathbf{F}_{oj}^i) &= u_j \mathbf{r}_{ij}^T (\mathbf{F}_{gj} - \mathbf{F}_{oi}^j).\end{aligned}$$

Not surprisingly, the set Z_i is depended on the current positions \mathbf{r}_i , \mathbf{r}_j and the goal locations \mathbf{q}_{gi} , \mathbf{q}_{gj} . The Zero condition reduces to $(\mathbf{F}_{gi} + \mathbf{F}_{gj}) = \mathbf{0}$, which corresponds to current positions $\mathbf{r}_i(t)$, $\mathbf{r}_j(t)$ and goal locations \mathbf{r}_{gi} , \mathbf{r}_{gj} lying on the same line. Then, the set of initial conditions (positions) from which agents' trajectories converge to the set Z_i is confined on \mathbb{R} , i.e., on a lower dimensional manifold, and as thus is of measure zero. The same analysis holds along the switching surface $T_i(t)$, yielding exactly the same condition as before regarding on the appearance of Zero points.

The case of $N > 2$ agents can be treated accordingly. Consider an agent i lying at distance $d_{im} \leq d_c$ w.r.t. $M \leq (N - 1)$ agents $m \neq i$. The vector field \mathbf{F}_i^* includes the repulsive effect \mathbf{F}_{om}^i of all M connected agents. To check whether undesired singularities appear, one needs to consider the norm $\|\mathbf{F}^i\|$ in the blending region \mathcal{D}_i . The analytical expression is more involved compared to the $N = 2$ case. To make the probability of more than one agents lying in the blending region \mathcal{D}_i as low as possible, one can define the width $d_c - d_r \rightarrow 0$. Define also:

$$S_{im}(t) : \{\mathbf{r}_i(t), \mathbf{r}_m(t) \in \mathbb{R}^2 \mid \|\mathbf{r}_i(t) - \mathbf{r}_m(t)\| - d_c = 0\}$$

the $M \leq (N - 1)$ switching surfaces of agent i w.r.t. its neighbors m . The conditions on the appearance of Zero points around each switching surface read:

$$\nabla S_{im}^- \mathbf{f}(\mathbf{r}_i, \mathbf{r}_m) = \nabla S_{im}^+ \mathbf{f}(\mathbf{r}_i, \mathbf{r}_m) = 0, \forall m \in \{1, \dots, N\}.$$

This results in $\frac{NM}{2}$ switching surfaces, since for any pair of agents (i, m) it holds that: $S_{im} = S_{mi}$, and NM Zeno conditions.

Now, note that the $\frac{NM}{2}$ Zeno conditions $S_{im}^- \mathbf{f}(\mathbf{r}_i, \mathbf{r}_m) = 0$ introduce $2 \frac{NM}{2} = NM$ unknown terms of the form $\mathbf{r}_{im}^T \mathbf{F}_{gi}$, $\mathbf{r}_{im}^T \mathbf{F}_{gm}$.

In the same spirit, the $\frac{NM}{2}$ Zeno conditions $S_{im}^+ \mathbf{f}(\mathbf{r}_i, \mathbf{r}_m) = 0$ additionally introduce $\frac{NM}{2}(M - 1)2 = NM(M - 1)$ unknown terms of the form $\mathbf{r}_{im}^T \mathbf{F}_{ok}^i$, $\mathbf{r}_{im}^T \mathbf{F}_{ok}^m$.

In total, one has NM^2 unknown terms and NM equations. Given that the N goal locations $\mathbf{r}_{gi}, \mathbf{r}_{gm}, \dots$, are known, the number of unknown terms reduces to $NM^2 - NM = NM(M - 1)$. To have as many equations as unknown terms, it should hold that $M - 1 = 1 \Rightarrow M = 2$. This implies that each agent $i \in \{1, \dots, N\}$ is connected with at most $M = 2$ agents; note that this is irrespective of the total number of agents N . Then, the geometric conditions which result in Zeno points are given as the solutions of the resulting linear system; these solutions express NM relations of the form $\mathbf{r}_{im}^T \mathbf{F}_{ok}^i$, $\mathbf{r}_{im}^T \mathbf{F}_{ok}^m$, which dictate the Zeno points, i.e., the Zeno positions among the N agents. Then, the set of initial conditions from which the agents converge to these Zeno positions are confined to a lower dimensional manifold, since they correspond to initial positions confined on a line, and to a specific initial orientation for each agent, and as thus are of measure zero.

Finally, let us note that the case of $M > 2$ neighbors is not of interest for the proposed algorithm, as each agent i makes the avoidance decision w.r.t. the worst-case neighbor agent, i.e., w.r.t. the agent which is more susceptible to collision. This is realized via considering the safe velocity $u_{i|m}$ w.r.t. each neighbor agent m and taking the minimum over safe velocities in the definition of the linear velocity control law (30a). The maximum function is defined to ensure that each agent i will never be forced to move with negative linear velocity, i.e., backwards; this is to ensure that there is no possibility of back-to-back colliding agents.

In summary, the motion of each agent i remains collision-free w.r.t. its neighbor agents $j \in \mathcal{N}_i$ under the control law (30), and each agent i converges to its goal location \mathbf{q}_{gi} almost globally, except for a set of initial configurations of measure zero. This completes the proof. ■

Remark 10: Theorem 5 justifies that the set of initial conditions for which the multi-robot system exhibits Zeno trajectories (chattering across a switching surface for infinite amount of time) which result in robots getting stuck away from their goals, is of measure zero. To avoid sliding along a switching surface, which can be seen as “finite-time chattering”, one can employ

hysteresis logics [45].

B. Simulation Results

We consider $N = 30$ agents which are moving towards their goal locations (depicted with square markers) starting from goal positions (depicted with cross markers) while avoiding collisions, see the resulting paths in Fig. ???. The goal locations are defined sufficiently far apart so that the communication regions do not overlap when agents lie on their goal locations.

VI. CONCLUSIONS

This paper presented a novel methodology for the motion planning of unicycle robots in environments with obstacles, with extensions to the collision avoidance in multi-agent systems. The method is based on a family of vector fields whose integral curves exhibit attractive or repulsive behavior depending on the value of a parameter. It was shown that attractive-to-the-goal and repulsive-around-obstacles vector fields can be suitably blended in order to yield almost global feedback motion plans in environments with circular obstacles. The case of collision avoidance under local sensing/communication in multi-agent scenarios was also treated. No parameter tuning is needed in order to avoid local minima, as needed in similar methods which are based on scalar (potential) functions. Current work focuses on the definition of vector fields encoding input constraints, such as curvature bounds, which may be more appropriate for aircraft and car-like vehicles.

REFERENCES

- [1] L. E. Parker, "Path planning and motion coordination in multiple mobile robot teams," in *Encyclopedia of Complexity and System Science*, R. A. Meyers, Ed. Springer, 2009.
- [2] H. Kress-Gazit, G. E. Fainekos, and G. J. Pappas, "Temporal-logic-based reactive mission and motion planning," *IEEE Transactions on Robotics*, vol. 25, no. 6, pp. 1370–1381, Dec. 2009.
- [3] A. Bhatia, M. R. Maly, L. E. Kavraki, and M. Y. Vardi, "A multi-layered synergistic approach to motion planning with complex goals," *IEEE Robotics and Automation Magazine*, vol. 18, no. 3, pp. 55–64, 2011.
- [4] W. Ren and Y. Cao, "Overview of recent research in distributed multi-agent coordination," in *Distributed Coordination of Multi-agent Networks*, ser. Communications and Control Engineering. Springer-Verlag, 2011, ch. 2, pp. 23–41.
- [5] D. Panagou, D. M. Stipanović, and P. G. Voulgaris, "Vision-based dynamic coverage control for nonholonomic agents," in *Proc. of the 53rd IEEE Conference on Decision and Control*, Los Angeles, CA, Dec. 2014, p. to appear.
- [6] D. Panagou and K. J. Kyriakopoulos, "Viability control for a class of underactuated systems," *Automatica*, vol. 49, no. 1, pp. 17–29, Jan. 2013.

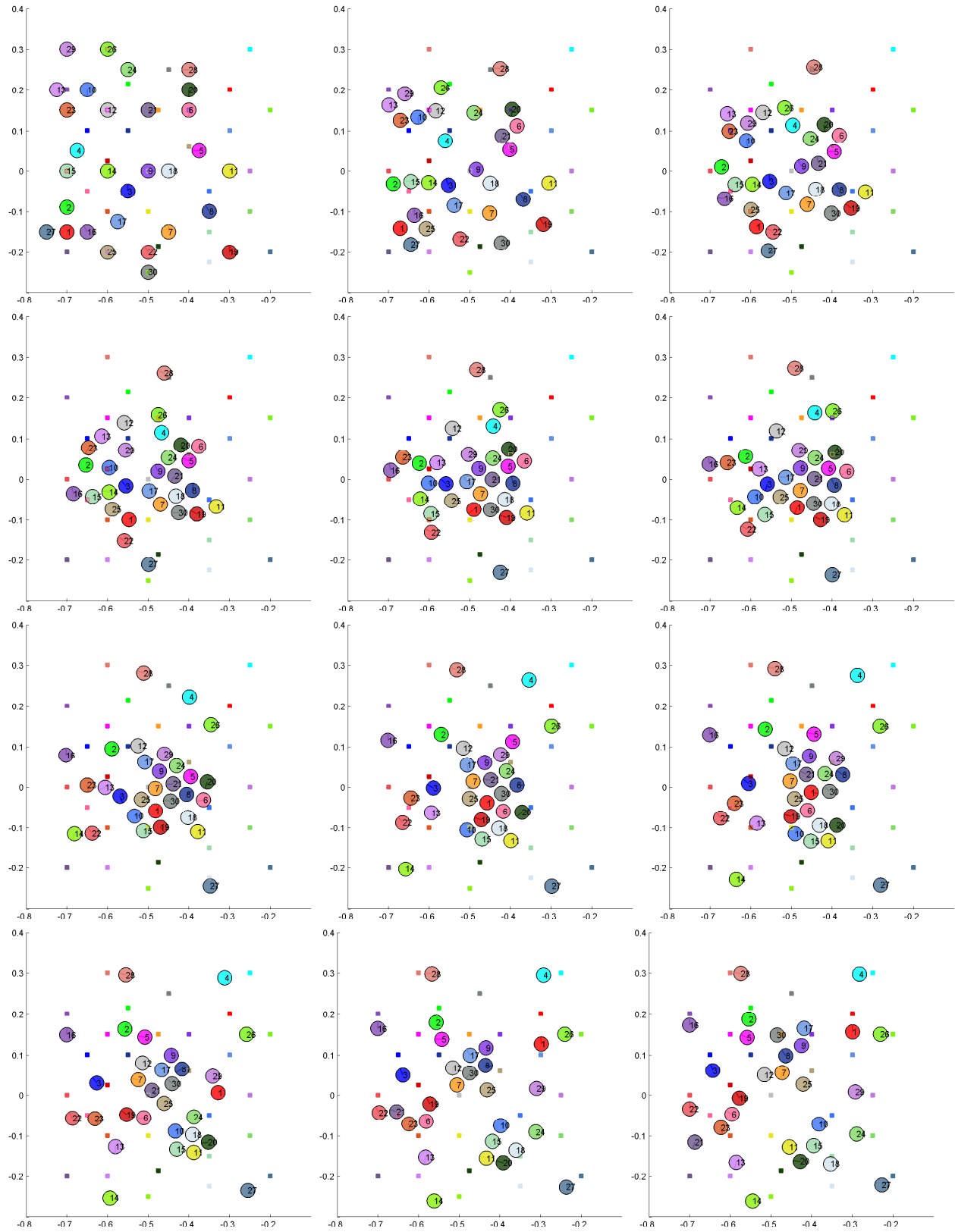


Fig. 7. Collision-free motion of 30 nonholonomic agents under the proposed control strategy.

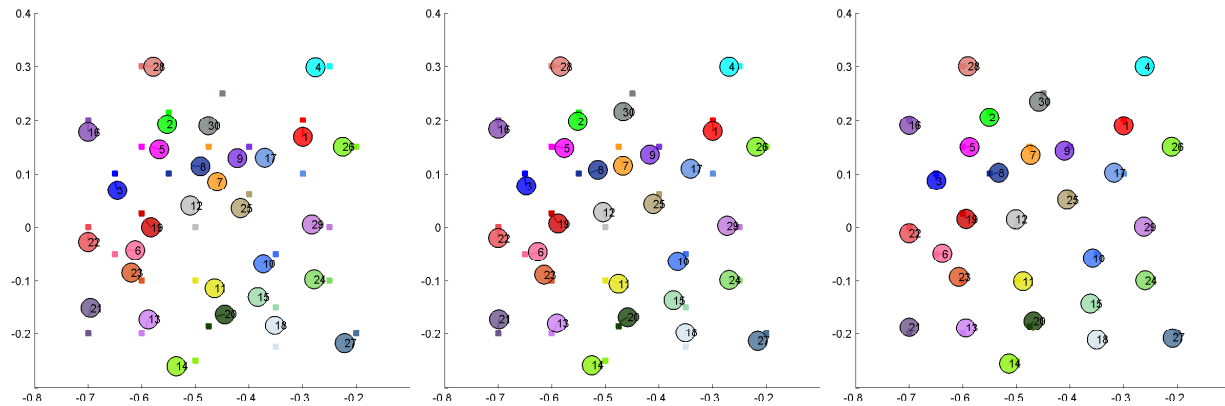


Fig. 8. Collision-free motion of 30 nonholonomic agents under the proposed control strategy (Continued).

- [7] G. Leitmann and J. Skowronski, "Avoidance control," *Journal of Optimization Theory and Applications*, vol. 23, pp. 581–591, Dec. 1977.
- [8] O. Khatib, "Real-time obstacle avoidance for manipulators and mobile robots," *The International Journal of Robotic Research*, vol. 5, no. 1, pp. 90–98, Spring, 1986.
- [9] E. G. Hernandez-Martinez and E. Aranda-Bricaire, "Convergence and collision avoidance in formation control: A survey of the artificial potential functions approach," in *Multi-Agent Systems - Modeling, Control, Programming, Simulations and Applications*, F. Alkhateeb, E. A. Maghayreh, and I. A. Doush, Eds. InTech, 2011, ch. 6, pp. 103–126.
- [10] D. M. Stipanović, C. J. Tomlin, and G. Leitmann, "Monotone approximations of minimum and maximum functions and multi-objective problems," *Applied Mathematics and Optimization*, vol. 66, pp. 455–473, 2012.
- [11] E. Rimon and D. Koditschek, "Exact robot navigation using artificial potential functions," *IEEE Transactions on Robotics and Automation*, vol. 8, no. 5, pp. 501–518, Oct. 1992.
- [12] C. I. Connolly, J. B. Burns, and R. Weiss, "Path planning using Laplace's equation," in *Proc. of the 1990 IEEE Int. Conf. on Robotics and Automation*, May 1990, pp. 2102–2106.
- [13] P. Szulczyński, D. Pazderski, and K. Kozłowski, "Real-time obstacle avoidance using harmonic potential functions," *Journal of Automation, Mobile Robotics and Intelligent Systems*, vol. 5, no. 3, pp. 59–66, 2011.
- [14] H. J. S. Feder and J.-J. E. Slotine, "Real-time path planning using harmonic potentials in dynamic environments," in *Proc. of the 1997 IEEE Int. Conf. on Robotics and Automation*, Albuquerque, New Mexico, Apr. 1997, pp. 874–881.
- [15] S. Waydo and R. M. Murray, "Vehicle motion planning using stream functions," in *Proc. of the 2003 IEEE Int. Conf. on Robotics and Automation*, Taipei, Taiwan, Sep., pp. 2484–2491.
- [16] A. D. Luca and G. Oriolo, "Local incremental planning for nonholonomic mobile robots," in *Proc. of the 1994 IEEE Int. Conf. on Robotics and Automation*, May 1994, pp. 104–110.
- [17] S. R. Lindemann and S. M. LaValle, "Simple and efficient algorithms for computing smooth, collision-free feedback laws over given cell decompositions," *The International Journal of Robotics Research*, vol. 28, no. 5, pp. 600–621, 2009.
- [18] T. Liddy, T.-F. Lu, P. Lozo, and D. Harvey, "Obstacle avoidance using complex vector fields," in *Proc. of the 2008 Australasian Conference on Robotics and Automation*, Canberra, Australia, Dec. 2008.
- [19] E. G. Hernández-Martínez and E. Aranda-Bricaire, "Multi-agent formation control with collision avoidance based on discontinuous vector fields," in *Proc. of the 35th Annual Conf. of IEEE Industrial Electronics*, Nov. 2009, pp. 2283–2288.

- [20] W. Dixon, T. Galluzo, G. Hu, and C. Crane, "Adaptive velocity field control of a wheeled mobile robot," in *Proc. of Fifth Int. Workshop on Robot Motion and Control*, Jun. 2005, pp. 145–150.
- [21] M. Mesbahi and M. Egerstedt, *Graph Theoretic Methods in Multiagent Networks*. Princeton University Press, 2010.
- [22] W. Ren, R. W. Beard, and E. M. Atkins, "Information consensus in multi-vehicle cooperative control," *IEEE Control Systems Magazine*, vol. 27, no. 2, pp. 71–82, apr 2007.
- [23] R. Olfati-Saber, J. A. Fax, and R. M. Murray, "Consensus and cooperation in networked multi-agent systems," *Proceedings of the IEEE*, vol. 97, no. 1, pp. 215–233, 2007.
- [24] D. V. Dimarogonas and K. J. Kyriakopoulos, "Connectedness preserving distributed swarm aggregation for multiple kinematic robots," *IEEE Transactions on Robotics*, vol. 24, no. 5, pp. 1213–1223, Oct. 2008.
- [25] S. G. Loizou and K. J. Kyriakopoulos, "Navigation of multiple kinematically constrained robots," *IEEE Transactions on Robotics*, vol. 24, no. 1, pp. 221–231, Feb. 2008.
- [26] P. Lin, Y. Jia, and L. Li, "Distributed robust h_∞ consensus control in directed networks of agents with time-delay," *Systems & Control Letters*, vol. 57, pp. 643–653, 2008.
- [27] J. Mei, W. Ren, and G. Ma, "Distributed containment control for lagrangian networks with parametric uncertainties under a directed graph," *Automatica*, vol. 48, pp. 653–659, 2012.
- [28] Z. Qu, C. Li, and F. Lewis, "Cooperative control with distributed gain adaptation and connectivity estimation for directed networks," *International Journal of Robust and Nonlinear Control*, 2012.
- [29] J. liang Zhang, D. lian Qi, and M. Yu, "A game theoretic approach for the distributed control of multi-agent systems under directed and time-varying topology," *International Journal of Control, Automation, and Systems*, vol. 12, no. 4, pp. 749–758, 2014.
- [30] Z. Li, G. Wen, Z. Duan, and W. Ren, "Designing fully distributed consensus protocols for linear multi-agent systems with directed graphs," *IEEE Transactions on Automatic Control*, to appear, 2014. [Online]. Available: <http://arxiv.org/abs/1312.7377v2>
- [31] W. Ren, "On consensus algorithms for double-integrator dynamics," in *Proc. of the 46th Conference on Decision and Control*, New Orleans, LA, USA, Dec. 2007, pp. 2295–2300.
- [32] K. Liu, G. Xie, W. Ren, and L. Wang, "Consensus for multi-agent systems with inherent nonlinear dynamics under directed topologies," *Systems & Control Letters*, vol. 62, no. 2, pp. 152–162, Feb. 2013.
- [33] D. Panagou, H. G. Tanner, and K. J. Kyriakopoulos, "Control of nonholonomic systems using reference vector fields," in *Proc. of the 50th IEEE Conf. on Decision and Control and European Control Conf.*, Orlando, FL, Dec. 2011, pp. 2831–2836.
- [34] M. Henle, *A Combinatorial Introduction to Topology*. Dover Publications, 1994.
- [35] D. Panagou, "Motion planning and collision avoidance using non-gradient navigation vector fields. Technical Report." [Online]. Available: www.arxiv.org
- [36] D. Panagou and V. Kumar, "Cooperative visibility maintenance for leader-follower formations in obstacle environments," *IEEE Transactions on Robotics*, vol. 30, no. 4, pp. 831–844, Aug. 2014.
- [37] D. Panagou, D. M. Stipanović, and P. G. Voulgaris, "Multi-objective control for multi-agent systems using Lyapunov-like barrier functions," in *Proc. of the 52nd IEEE Conference on Decision and Control*, Florence, Italy, Dec. 2013, pp. 1478–1483.
- [38] S. Maniatiopoulos, D. Panagou, and K. J. Kyriakopoulos, "A MPC scheme for the navigation of a nonholonomic vehicle with field-of-view constraints," in *Proc. of the 2013 American Control Conf.*, Washington DC, USA, Jun. 2013, pp. 3967–3972.

- [39] D. Panagou, “Motion planning and collision avoidance using navigation vector fields,” in *Proc. of the 2014 IEEE International Conference on Robotics and Automation*, Hong Kong, China, Jun. 2014, pp. 2513–2518.
- [40] W. M. Boothby, *An Introduction to Differentiable Manifolds and Riemannian Geometry - 2nd Edition*. Academic Press, 1986.
- [41] J. M. Lee, *Introduction to Smooth Manifolds*. Springer, 2002.
- [42] X. Tricoche, G. Scheuermann, and H. Hagen, “A topology simplification method for 2D vector fields,” in *Proc. of Visualization 2000*, Salt Lake City, UT, USA, Oct., pp. 359–366.
- [43] A. D. Ames and S. Sastry, “Characterization of Zeno behavior in hybrid systems using homological methods,” in *Proc. of the 2005 American Control Conf.*, Portland, OR, USA, Jun. 2005, pp. 1160–1165.
- [44] F. Ceragioli, “Finite valued feedback laws and piecewise classical solutions,” *Nonlinear Analysis*, vol. 65, no. 5, pp. 984–998, 2006.
- [45] D. Liberzon, *Switching in Systems and Control*. Birkhauser Boston, 2003.

APPENDIX

Here we present some preliminary ideas on the extension of the method to polygonal environments.

Consider the pattern of the integral curves for $\lambda < -1$, shown in Fig. 9. The repulsive nature of the integral curves w.r.t. the axis the vector \mathbf{p} lies on can be used to define a repulsive flow w.r.t. each side of polygonal obstacles, as shown in Fig. 10. The effect of the repulsive flows can be confined around the polygonal obstacle using blending mechanisms as those presented in Section 4. Identifying sufficient minimum clearance around the obstacles which guarantees the almost global convergence of the integral curves to a goal configuration in such a polygonal environment is currently ongoing work, and beyond the scope and the length of the current paper.

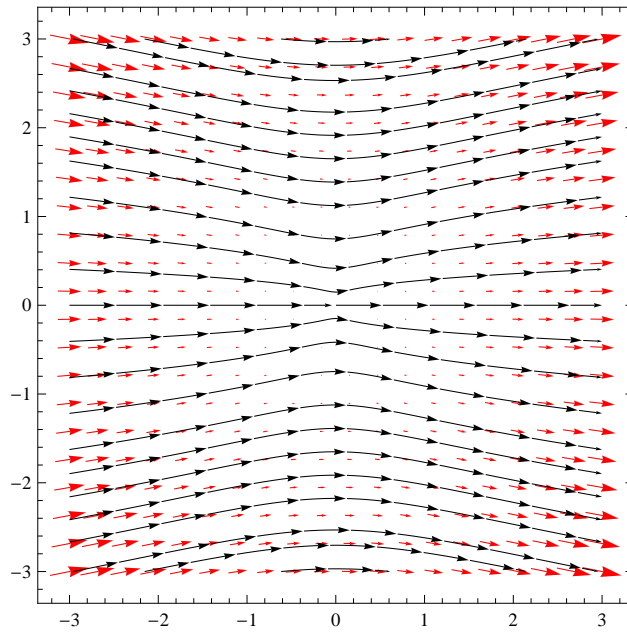


Fig. 9. The integral curves for $\lambda = -1, p_x = -1, p_y = 0$.

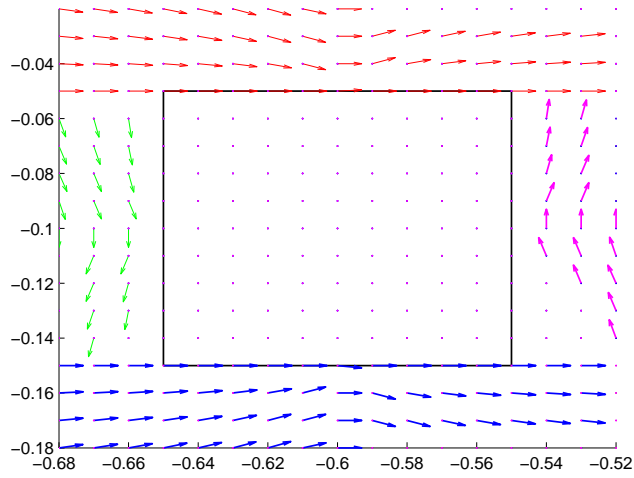


Fig. 10. Integral curves around a polygonal obstacle.